



Minerva Access is the Institutional Repository of The University of Melbourne

Author/s:

Schmidt, TL;Swan, T;Chung, J;Karl, S;Demok, S;Yang, Q;Field, MA;Muzari, MO;Ehlers, G;Brugh, M;Bellwood, R;Horne, P;Burkot, TR;Ritchie, S;Hoffmann, AA

Title:

Spatial population genomics of a recent mosquito invasion

Date:

2021-03-01

Citation:

Schmidt, T. L., Swan, T., Chung, J., Karl, S., Demok, S., Yang, Q., Field, M. A., Muzari, M. O., Ehlers, G., Brugh, M., Bellwood, R., Horne, P., Burkot, T. R., Ritchie, S. & Hoffmann, A. A. (2021). Spatial population genomics of a recent mosquito invasion. *Molecular Ecology*, 30 (5), pp.1174-1189. <https://doi.org/10.1111/mec.15792>.

Persistent Link:

<https://hdl.handle.net/11343/298151>

1
2
3
4
5
6
7
8
9
10
11
12
13
14
15
16
17
18
19
20
21
22
23
24

DR. THOMAS LUDOVIC SCHMIDT (Orcid ID : 0000-0003-4695-075X)

PROF. ARY HOFFMANN (Orcid ID : 0000-0001-9497-7645)

Article type : Original Article

Spatial population genomics of a recent mosquito invasion

Thomas L Schmidt*¹, T. Swan*^{2,3}, Jessica Chung^{1,4}, Stephan Karl^{2,5}, Samuel Demok⁵, Qiong Yang¹,
Matt A Field^{2,6}, Mutizwa Odwell Muzari⁷, Gerhard Ehlers⁷, Mathew Brugh⁷, Rodney Bellwood⁷,
Peter Horne⁷, Thomas R Burkot², Scott Ritchie^{3,8}, Ary A Hoffmann¹

¹ Pest and Environmental Adaptation Research Group, Bio21 Institute, School of BioSciences, University of Melbourne, Parkville, VIC, Australia

² Australian Institute of Tropical Health and Medicine, James Cook University, Cairns, QLD, Australia

³ College of Public Health, Medical and Veterinary Sciences, James Cook University, Cairns, QLD, Australia

⁴ Melbourne Bioinformatics, University of Melbourne, Parkville, Victoria, Australia

⁵ Vector Borne Diseases Unit, Papua New Guinea Institute of Medical Research, Madang, Papua New Guinea

⁶ John Curtin School of Medical Research, Australian National University, Canberra, ACT

⁷ Medical Entomology, Tropical Public Health Services Cairns, Cairns and Hinterland Hospital & Health Services, Cairns, QLD, Australia

⁸ Institute of Vector-Borne Disease, Monash University, Clayton, VIC, 3800, Australia

This is the author manuscript accepted for publication and has undergone full peer review but has not been through the copyediting, typesetting, pagination and proofreading process, which may lead to differences between this version and the [Version of Record](#). Please cite this article as [doi: 10.1111/MEC.15792](https://doi.org/10.1111/MEC.15792)

This article is protected by copyright. All rights reserved

25 * equal contributions

26 Contact: tom.schmidt@unimelb.edu.au

27 Running title: Population genomics of a recent invasion

28 Abstract

29 Population genomic approaches can characterise dispersal across a single generation through to
30 many generations in the past, bridging the gap between individual movement and
31 intergenerational gene flow. These approaches are particularly useful when investigating
32 dispersal in recently altered systems, where they provide a way of inferring long-distance
33 dispersal between newly established populations and their interactions with existing
34 populations. Human-mediated biological invasions represent such altered systems which can be
35 investigated with appropriate study designs and analyses. Here we apply temporally-restricted
36 sampling and a range of population genomic approaches to investigate dispersal in a 2004
37 invasion of *Aedes albopictus* (the Asian tiger mosquito) in the Torres Strait Islands (TSI) of
38 Australia. We sampled mosquitoes from 13 TSI villages simultaneously and genotyped 373
39 mosquitoes at genome-wide single nucleotide polymorphisms (SNPs): 331 from the TSI, 36 from
40 Papua New Guinea (PNG), and 4 incursive mosquitoes detected in uninvaded regions. Within
41 villages, spatial genetic structure varied substantially but overall displayed isolation by distance
42 and a neighbourhood size of 232–577. Close kin dyads revealed recent movement between
43 islands 31–203 km apart, and deep learning inferences showed incursive *Ae. albopictus* had
44 travelled to uninvaded regions from both adjacent and non-adjacent islands. Private alleles and
45 a coancestry matrix indicated direct gene flow from PNG into nearby islands. Outlier analyses
46 also detected four linked alleles introgressed from PNG, with the alleles surrounding 12
47 resistance-associated cytochrome P450 genes. By treating dispersal as both an
48 intergenerational process and a set of discrete events, we describe a highly interconnected
49 invasive system.

50

51

52

53 **Keywords:** dispersal, *Aedes albopictus*, adaptive introgression, genetic invasion, kinship,
54 **biological invasion**

55

56

57 Introduction

58

59 Population genetics has traditionally treated dispersal as an intergenerational process, but one
60 that is nevertheless derived from the movement of individual organisms within each generation
61 (Wright, 1943). Intergenerational dispersal describes how organisms distributed across
62 geographical space are connected through time via a spatial pedigree (Bradburd & Ralph, 2019),
63 and can be summarised at a population level by the mean distance between parent and
64 offspring. Population genomic approaches applied to wild populations increasingly provide the
65 power needed to detect dispersal across fine temporal scales down to single generations, which
66 can reveal movement patterns at correspondingly fine spatial scales (Combs, Puckett,
67 Richardson, Mims, & Munshi-South, 2018; Jasper, Schmidt, Ahmad, Sinkins, & Hoffmann, 2019;
68 Trense et al., 2020). Spatial genomic studies conducted across a restricted temporal range may
69 also help shed new light on adaptive processes such as the spread of advantageous alleles
70 through wild populations (Endersby-Harshman et al., 2020; Fitzpatrick et al., 2010; Péliissié,
71 Crossley, Cohen, & Schoville, 2018) and local adaptation in microgeographically structured
72 environments (Yadav, Stow, & Dudaniec, 2020).

73 Individuals connected through recent generations of the spatial pedigree will be close kin, with
74 full-sibs and half-sibs separated by a single generation and first cousins by two. Close kin dyads
75 can be identified using genomics, and the spatial distribution of kin has been used in recent
76 studies to detect dispersal over fine temporal scales (Combs et al., 2018; Escoda, Fernández-
77 González, & Castresana, 2019; Escoda, González-Esteban, Gómez, & Castresana, 2017; Fountain
78 et al., 2018; Jasper et al., 2019; Schmidt, Filipović, Hoffmann, & Rašić, 2018; Trense et al., 2020).
79 Dispersal inferences from close kin treat dispersal as a set of discrete events reflecting specific
80 acts of individual movement, making them particularly valuable for investigating dispersal
81 through regions of genetic similarity, such as where populations have only recently become
82 isolated (Escoda et al., 2019, 2017) or where a population has been sampled continuously
83 across a range (Combs et al., 2018; Jasper et al., 2019; Schmidt et al., 2018; Trense et al., 2020).
84 As kinship-based approaches assess recent movement, they are ideally applied to systems
85 which have been subject to recent change, such as biological invasions or threatened species in
86 disturbed habitats.

87 While the past 1-2 generations of dispersal represent very recent movement, population
88 genomics has also been used to detect intragenerational dispersal, which has traditionally been
89 investigated by directly observing the movement of individuals (Harrington et al., 2005; Schultz
90 & Crone, 2001). Examples of this approach include tracing individual invasive species incursions
91 (“incursions”) to their population of origin (M. Z. Chen et al., 2020; Schmidt, Chung, van Rooyen,
92 et al., 2020; Schmidt et al., 2019). Although such studies require sampling across broad scales
93 they are a useful way of detecting long-distance dispersal, which is difficult to investigate but
94 can have important evolutionary consequences (Gillespie et al., 2012; Waters, Fraser, & Hewitt,
95 2013). Note that when incursive individuals are intercepted, there is no ‘dispersal’ in the
96 intergenerational sense, but these movements are nevertheless important components of life-
97 histories and food webs (Howard, 1960).

98 Recent human-mediated biological invasions are complex spatial processes that require careful
99 investigation. In recent invasions, high regional coancestry throughout the invaded region will

100 make the analysis of genetic structure alone insufficient for evaluating movement (Fitzpatrick,
101 Fordyce, Niemiller, & Reynolds, 2012). Additionally, invasive species, defined here as any taxon
102 which rapidly spreads (following Cristescu (2015)), frequently exhibit stratified dispersal, in
103 which short-range active movement by the organism and long-range passive transportation by
104 humans operate together across a range of spatial scales within a generation (Hengeveld, 1989;
105 Sharov & Liebhold, 1998). Long-range dispersal can be traced within invaded regions or from
106 distant origins (Schmidt, Chung, Honnen, Weeks, & Hoffmann, 2020; Sherpa et al., 2019), and
107 can operate alongside short-range dispersal to spread adaptive alleles into and through invasive
108 populations (Endersby-Harshman et al., 2020; Pélissié et al., 2018). Applying intragenerational
109 and kinship-based dispersal methods to recent invasions may help detect recent movement
110 across fine and broad spatial scales, with dispersal between invaded regions revealed through
111 close kin and intragenerational incursions into uninvaded regions traced to their source.

112 Here we use spatial population genomics to investigate an invasion of *Aedes albopictus* (Asian
113 tiger mosquito) in the Torres Strait Islands (TSI), Australia, sampled ~14 years after
114 colonisation. The Torres Strait lies between the northernmost point of the Australian mainland
115 (Cape York) and Papua New Guinea (PNG) (Fig 1 inset). The region contains over 100 islands, of
116 which 18 are inhabited communities (<http://www.tsra.gov.au/the-torres-strait/community-profiles#TS%20Communities>) and which we refer to here as 'villages' to distinguish from
117 ecological communities. *Aedes albopictus* was first detected in the TSI in 2004 (Ritchie et al.,
118 2006), and an insecticide-focussed elimination program began shortly thereafter. Logistical
119 difficulties and recurrent reinvasion risks led to the abandonment of this program in 2008 in
120 favour of a containment strategy, in which a *cordon sanitaire* was imposed to regulate the
121 movement of people and goods between the invaded islands of the Torres Strait and the
122 uninvaded 'inner' islands of Ngurapai (Horn) and Waiben (Thursday) (Muzari et al., 2017; van
123 den Hurk et al., 2016). Ngurapai and Waiben serve as commercial hubs connecting the TSI and
124 the Australian mainland, and the *cordon sanitaire* approach has likely helped prevent incursion
125 of *Ae. albopictus* onto the mainland of Australia through the Torres Strait route though it
126 continues to vector dengue outbreaks in the TSI (Muzari et al., 2017). *Aedes albopictus*
127

128 incursions continue to be detected at ports on the Australian mainland and have been traced to
129 locations in East and Southeast Asia that have strong trade links to Australia (Schmidt, Chung,
130 van Rooyen, et al., 2020). Previous investigations of TSI *Ae. albopictus* using mtDNA and
131 microsatellites indicated high coancestry with Indonesian *Ae. albopictus* (Beebe et al., 2013;
132 Maynard et al., 2017). Additional observations of spatially and temporally variable genetic
133 structure within the TSI could reflect high regional gene flow following local founder events
134 (Maynard et al., 2017).

135 While Indonesia is the likely source of the initial invasion into the TSI, over 5,000 boat journeys
136 are made each year between TSI and PNG (Mcfarlane, 1998), indicating the potential for gene
137 flow across this border. When gene flow takes place after an initial invasion it can operate as a
138 'genetic invasion' if it interferes with control strategies, such as through introgression of alleles
139 conferring insecticide resistance (Endersby-Harshman et al., 2020; Riveron et al., 2013; Schmidt
140 et al., 2019). Although the TSI was likely invaded from Indonesia via a 'stepping-stone' in the
141 Southern Fly region of PNG (Beebe et al., 2013), the absence of *Ae. albopictus* in Southern Fly in
142 the late 1990s (Johansen et al., 2000) and its present genetic similarity to the TSI (Maynard et
143 al., 2017) indicates that the invasion of the TSI and Southern Fly regions happened
144 contemporaneously from Indonesia. PNG *Ae. albopictus* from outside the Southern Fly region
145 are genetically distinct from Indonesian *Ae. albopictus* (Maynard et al., 2017) and gene flow
146 from this PNG background should be readily detectable.

147 This investigation covers a range of spatial scales from 10s of metres to 1000s of kilometres, and
148 temporal scales from a single generation to ~100 generations in the past. Within the TSI, where
149 coancestry is high, we focus on dispersal in the immediate past, covering both short-range
150 active flight within islands and long-range passive transportation between islands, including
151 incursions past the *cordon sanitaire*. At broader spatial scales, we use a panel of differentiated
152 genotypes from other locations including nearby PNG to investigate earlier patterns of gene
153 flow into the TSI. Our specific aims are: (i) to investigate the spatial structure of passive
154 dispersal, and whether it occurs only between nearby locations or distant locations as well; (ii)

155 to ascertain whether new genetic structure among islands has developed since previous
156 investigation (Maynard et al., 2017); and (iii) to determine whether gene flow has occurred from
157 PNG into the TSI, including the spread of putatively adaptive alleles. Through this, we show how
158 stratified dispersal operates in this system and how long-range dispersal can assist the rapid
159 invasion of new regions and the spread of advantageous alleles through established
160 populations. The rapid spread of *Ae. albopictus* and its capacity for long-distance invasion make
161 studies of its dispersal globally relevant (Goubert et al., 2017; Schmidt, Chung, Honnen, et al.,
162 2020; Sherpa et al., 2019).

163

164

165 Materials and methods

166 Sample acquisition and genotyping

167 We analysed *Ae. albopictus* single nucleotide polymorphism (SNP) data from multiple sources.
168 These included new mosquito samples collected from the Torres Strait Islands (TSI) and Papua
169 New Guinea (PNG) as well as sequence data collected previously from across the Indo-Pacific
170 region. We use the alphabetical key (A-L) in Fig 1 in all references to TSI villages.

171 Sampling in the invaded regions of the TSI took place at two time points. The first involved
172 cross-sectional collections from 13 villages on 12 islands sampled between 2018-04-24 and
173 2018-05-04 (Fig 1). On Moa Island, two villages were sampled (B:St Pauls and C:Kubin). By
174 restricting the temporal range of sampling, it is possible to undertake investigations within and
175 between villages that require data at a fine temporal scale (i.e. within 1–2 generations), such as
176 kinship analysis. Within each village, researchers selected and georeferenced sampling points
177 where they collected adult *Ae. albopictus* with sweep-nets. Sampling points were separated by
178 at least 100 m where possible (maximum 3,297 m), and each village had 15–20 sampling points

179 except Dauan which had 7 (Fig 1: red crossed square). *Aedes albopictus* were preserved in 100%
180 ethanol prior to DNA extraction. A second TSI sampling event took place on I:Masig between
181 2019-03-28 and 2019-04-08 at the same sampling points, serving as a temporal replicate. Village
182 maps and sampling point locations are detailed in Figures S1-S13.

183 In February 2019, we detected *Ae. albopictus* incursions on the island of Ngurapai, south of the
184 *cordon sanitaire* (see Fig 2). Four incursive *Ae. albopictus* adults were detected between 2019-
185 02-02 and 2019-02-09 during routine wet season surveillance (Figure S14) and the samples were
186 preserved for DNA extraction. Similar surveys, conducted with sweep nets in December 2018,
187 March 2019 and May 2019 did not detect any *Ae. albopictus* on the island.

188 A final set of samples was collected from PNG between 2018-08-02 and 2018-09-13 using
189 ovitraps deployed at several urban locations around the cities of Port Moresby (south coast) and
190 Madang (north coast). These were aggregated to produce one Port Moresby sample and one
191 Madang sample, with a maximum of two mosquitoes taken from each individual ovitrap to
192 reduce the likelihood of sampling close kin.

193 Samples were genotyped using a pipeline described previously (Schmidt, Chung, van Rooyen, et
194 al., 2020) and described in full in Text S1. Briefly, we used the double digest restriction site-
195 associated (ddRAD) sequencing protocol developed for *Ae. aegypti* (Rašić, Filipović, Weeks, &
196 Hoffmann, 2014) and validated in *Ae. albopictus* (Schmidt et al., 2017). Sequence reads were
197 processed in Stacks v2.41 (Catchen, Hohenlohe, Bassham, Amores, & Cresko, 2013), with
198 Bowtie2 v2.3.5.1 (Langmead & Salzberg, 2012) used to align reads to the AalbF2 genome
199 assembly (Palatini et al., 2020).

200 Sequence data were generated for 371 *Ae. albopictus*: 301 from the cross-sectional collections
201 on the invaded islands, 30 from the temporal replicate on I:Masig, 4 from the incursions past
202 the *cordon sanitaire*, and 18 from each of Madang and Port Moresby in PNG. We also included
203 sequence data from previous work (Schmidt, Chung, Honnen, et al., 2020; Schmidt, Chung, van
204 Rooyen, et al., 2020). This included sequences from Indonesia (Bali, Bandung and Jakarta) and

205 Timor-Leste, the proposed approximate origin of the initial TSI invasion (Beebe et al., 2013;
206 Maynard et al., 2017). We also added sequences from locations linked to Australian *Ae.*
207 *albopictus* incursions: China (Guangzhou), Japan, Singapore and Taiwan (Schmidt, Chung, van
208 Rooyen, et al., 2020). Finally, we included two Pacific Island locations from East of PNG: Fiji and
209 Vanuatu. These data were all reprocessed through the same bioinformatics pipeline.

210

211

212 Datasets and filtering

213 Genotypes were filtered with the Stacks v2.41 program Populations (Catchen et al., 2013),
214 VCFtools v0.1.16 (Danecek et al., 2011), and Beagle v4.1 (Browning & Browning, 2016).
215 Populations produced VCF files containing SNPs called in ≥ 0.75 of the mosquitoes from each
216 village, location or timepoint; VCFtools retained biallelic SNPs with minor allele count ≥ 3 (Linck
217 & Battey, 2019), depth of coverage ≥ 5 , and genotyped in $\geq 80\%$ of total mosquitoes; and Beagle
218 imputed and phased genotypes in 50,000 bp sliding windows with 3,000 bp overlap.

219 We first used Populations and VCFtools to detect close kin dyads (1st and 2nd order) within each
220 village. We used the *relatedness2* command in VCFtools to detect first-order (parental or full-
221 sib) and second-order (grandparental or half-sib) kin dyads, analysing each village separately.
222 This command uses the KING (Manichaikul et al., 2010) method of generating kinship
223 coefficients for pairwise relationship inference; accordingly, we used kinship coefficient cut-offs
224 of > 0.177 for first-order kin and > 0.088 for second order kin. Close kin dyads identified at this
225 step were used to help estimate kinship categories of dyads across villages (see 'Close kin across
226 villages' below).

227 For analysis within the TSI, we were cautious to avoid filtering bias caused by close kin and
228 uneven sample sizes (Puechmaille, 2016). Accordingly, we produced datasets of $n = 22$ for each
229 village, with 22 the maximum number of genotypes that ensured equal sample sizes after

230 removing close kin within and across villages (see Results). Kin were removed in order of missing
231 data, other genotypes were removed to maximise the geographical distribution of genotypes,
232 then by missing data. Datasets were imputed and phased with Beagle and hereafter called the
233 “Village22” datasets, each containing between 7,877–9,873 SNPs.

234 We also produced a dataset for the TSI region called “Region22” that contained all individuals
235 from the Village22 datasets, containing 26,085 SNPs. Tracing of incursions and gene flow from
236 PNG used this dataset where specified, with the incursive or PNG genotypes included. For
237 analyses using the additional Indo-Pacific genotypes, we included all non-incursive individuals
238 from the TSI including Dauan, with the temporal replicate from I:Masig excluded and with the
239 dataset left unimputed where indicated. This dataset contained 495 mosquitoes genotyped at
240 26,970 SNPs.

241

242

243 Population processes within the Torres Strait

244

245 *TSI genetic structure*

246 We investigated genetic structure in the TSI using sparse non-negative matrix factorisation
247 (sNMF) in the R package “LEA” (Frichot & François, 2015), run on the Region22 dataset. This
248 analysis estimates individual ancestry coefficients, assuming that individual genotypes are
249 produced from the admixture of K ancestral lineages. Previous research using microsatellites to
250 analyse samples from 2007–2015 found two main genetic lineages in the TSI (Maynard et al.,
251 2017). Accordingly, we ran 50 iterations of the sNMF with $2 \leq K \leq 4$ but used $K = 2$ for
252 visualisations to provide a direct comparison with this work.

253 We used Populations to calculate heterozygosity (H_o) and nucleotide diversity (π) at variant
254 sites and pairwise F_{ST} between all village samples. We used VCFtools to calculate Tajima's D in
255 10 Mbp windows, including the temporal replicate from I:Masig to reveal any changes over the
256 12 month period. We used the R package "hierfstat" (Goudet, 2005) to estimate global F_{ST} and
257 the population differentiation statistic D_{est} (Jost, 2008) among the 2018 samples.

258

259 ***Dispersal within villages***

260 Within TSI villages (< 3.5 km), dispersal is mostly by active flight through continuous habitat and
261 can be summarised by the parameter σ , which makes up the dispersal variance component of
262 neighbourhood size (N_w : Wright, 1946). N_w can be thought of as the effective number of *Ae.*
263 *albopictus* that make up a mosquito's breeding 'neighbourhood' when isolation by distance is
264 operating. The equation, $N_w = 4\pi \cdot \sigma^2 \cdot d$, provides a link between spatial patterns of genetic
265 differentiation and local demographic processes, connecting intergenerational dispersal (σ^2) to
266 the effective density of breeding adults within the dispersal area (d).

267 We used the Village22 datasets to investigate isolation by distance within each village. Mantel
268 tests (function mantel.randtest) ran in the R package "ade4" (Dray & Dufour, 2007) analysed
269 matrices of individual linear genetic distance and the natural logarithm of Haversine geographic
270 distance, using 9,999 permutations and Bonferroni correction to assess statistical significance.
271 Rousset's a (Rousset, 2000) provided genetic distance, calculated in SPAGeDI (Hardy &
272 Vekemans, 2002).

273 We estimated neighbourhood size (N_w : Wright, 1946) within all villages using the inverse of the
274 regression slope of pairwise genetic distance (Rousset's a) against the natural logarithm of
275 geographical distance (Rousset, 2000). As the linearity of this relationship may break down at
276 distances within the dispersal estimate σ , we omitted pairs < 50 m apart. The temporal replicate

277 from I:Masig was also omitted. The pairwise data used for Mantel tests were concatenated to
278 run a single linear regression on the 5325 within-village dyads.

279

280 ***Close kin across villages***

281 Having identified close kin dyads within villages, we applied a conservative process for detecting
282 kin across villages, which represent passive transportation by humans. First, we generated
283 kinship coefficients using PC-Relate (Conomos, Reiner, Weir, & Thornton, 2016), which controls
284 for genetic structure by conditioning the data with principal components (PCs). We ran PC-
285 Relate on the dataset containing all non-incursive individuals, first pruning SNPs by linkage
286 disequilibrium (R package “SNPRelate” (Zheng et al., 2012); using the snpgdsLDpruning function
287 with arguments, method = “composite” and ld.threshold = 0.2).

288 We generated kinship coefficients for all dyads within and across villages following three
289 different conditioning treatments: 3 PCs, 5 PCs, and 10 PCs. As a lower bound for determining
290 which dyads across villages could be considered to have a particular category of relatedness, we
291 used the lowest kinship coefficient observed among all close kin dyads within villages (see
292 Datasets and filtering).

293 For each dyad found across two villages, one individual (Sib-1) or its recent relative will have
294 dispersed to a new environment (Village-1) while the other (Sib-2) has stayed at the origin
295 (Village-2). Thus, Sib-1 and Sib-2 should both have higher coancestry with individuals from
296 Village-2 than those from Village-1, which should be reflected in higher average kinship with
297 Village-2. We estimated the direction of dispersal by comparing kinship coefficients of Sib-1 and
298 Sib-2 with each village, which allowed us to determine the origin (Village-2) and the destination
299 (Village-1). These differences were evaluated with t-tests.

300

301

302 Incursions past the *cordon sanitaire*

303 To estimate source locations of the four incursive *Ae. albopictus*, we used two complementary
304 methods in the programs assignPOP (K.-Y. Chen et al., 2018) and Locator (Battey, Ralph, & Kern,
305 2020). assignPOP treats each village as a population, and generates assignment probabilities to
306 each hypothetical population using a Monte Carlo assignment test with a support vector
307 machine predictive model. Locator makes no population-based assumptions, but uses
308 geolocations of individual genotypes to infer the spatial origin of each incursive using deep
309 learning. These analyses used the Region22 dataset, omitting the temporal replicate from
310 I:Masig.

311 Following Schmidt et al. (2019), we used the assignPOP function assign.X to generate posterior
312 probabilities of assignment from which we calculated ‘relative probabilities’ of assignment,
313 defined as the highest posterior probability divided by the second highest. Relative probability >
314 3 has previously been used as a cut-off for *Ae. albopictus* assignment at broad scales (Schmidt,
315 Chung, van Rooyen, et al., 2020).

316 To run Locator we first pruned SNPs by linkage disequilibrium using the snpgdsLDpruning
317 function in the R package “SNPRelate” (arguments, method = composite and ld.threshold = 0.2).
318 This dataset provided a point estimate of each incursive’s original location, and 1000 bootstrap
319 subsamples were run to provide confidence around these estimates. While Locator has options
320 for analysing SNPs in windows, our ddRADseq data were too sparse and the reference assembly
321 insufficient for this.

322 Before running final assignments, we first confirmed that each of the four incursives had an
323 origin in the TSI through an initial run of assignPOP using the dataset containing all non-
324 incursive Indo-Pacific genotypes. These results showed strong support for each incursive
325 mosquito having an origin in the TSI, with aggregated posterior assignment probabilities of
326 0.89–0.97 to the TSI and 0.11–0.03 to non-TSI locations (Table S1).

327

328 International gene flow into the Torres Strait

329 ***Genome-wide gene flow***

330 We used fineRADstructure (Malinsky, Trucchi, Lawson, & Falush, 2018) to investigate possible
331 coancestry between TSI *Ae. albopictus* and those from locations other than Indonesia or Timor-
332 Leste. We ran fineRADstructure with default settings on the dataset containing all non-incursive
333 Indo-Pacific genotypes, with the temporal replicate of I:Masig removed.

334 This analysis also helped clarify genetic relationships among genotypes in the broader region. To
335 assist with the visualisation of these relationships, we ran a PCA-UMAP analysis (Diaz-Papkovich,
336 Anderson-Trocme, Ben-Eghan, & Gravel, 2019) on the same dataset. PCA-UMAP used the first 4
337 PCs, projected in two dimensions via UMAP using 50 neighbours and a 0.5 minimum distance.

338 Using the Region22 dataset, we calculated the number of private alleles in each TSI village with
339 Populations, excluding the temporal replicate from I:Masig. This was then recalculated with the
340 two PNG samples (Port Moresby and Madang) included in filtering. By comparing the number of
341 private alleles in each village with and without the PNG samples, we assessed gene flow
342 between each village and PNG. Specifically, if fewer private alleles were recorded for a village
343 after the PNG samples were included in filtering, the “missing” alleles will be identical by state
344 and likely identical by descent in both PNG and that village. As these alleles are restricted to
345 specific villages, they are evidence of gene flow from PNG into each village directly.

346

347 ***Adaptive introgression***

348 While ddRAD data are typically too sparse to detect alleles under selection, they can be suitable
349 for detecting selective sweeps as shown by previous work on *Ae. aegypti* (Endersby-Harshman
350 et al., 2020). We looked for signs that advantageous alleles had spread into the TSI using a

351 three-step process: identifying genomic regions of interest, where multiple SNPs had irregular
352 structure consistent with linked selection; identifying genes within these genomic regions of
353 potential adaptive importance; and identifying the geographical origin of alleles at these SNPs.

354 We used the R packages *pcadapt* (Luu, Bazin, & Blum, 2017) and LEA (Frichot & François, 2015:
355 function *sNMF*) to detect SNPs with irregular structure. Analyses were run on the Region22
356 dataset. We ran *pcadapt* with a minimum allele frequency of 0.025 (≥ 15 allele copies present),
357 and obtained P-values from Mahalanobis distances. Genomic inflation factors for all runs were $<$
358 1.5. We ran *sNMF* using default parameters and 50 repetitions, and selected outliers by F_{ST} . For
359 each analysis, P-values were transformed using a Bonferroni correction, and we used a q-value
360 cut-off of 0.001. Only SNPs detected as outliers by both *pcadapt* and *sNMF* were considered. As
361 genotype imputation methods can introduce bias when imputing rare alleles (Shi et al., 2018),
362 we repeated the above methods without imputation in Beagle.

363 Within TSI *Ae. albopictus*, local demographic changes such as founder effects may have
364 eliminated genetic diversity in particular regions of the genome, which a genome scan may
365 incorrectly read as the result of a selective sweep (Hoban et al., 2016). For this reason, we
366 restricted our investigation to outlier regions that satisfied three conditions: (i) the region
367 contained multiple outlier SNPs spread across multiple RADtags within 1 Mbp; (ii) the region
368 contained one or more genes with products of plausible adaptive importance, such as
369 insecticide resistance; and (iii) the alleles at the specific outlier SNPs within the region were not
370 found in Indonesia (putative source of the TSI invasion) but were found in other populations
371 outside of the TSI. For (ii) we used Integrative Genomics Viewer (Robinson et al., 2011) to
372 visually explore the *Ae. albopictus* reference assembly. For (iii), we used the dataset containing
373 all non-invasive Indo-Pacific genotypes (N = 525), without imputation.

374

375

376 Results

377

378 Population processes within the Torres Strait

379 *TSI genetic structure*

380 Analysis of genetic structure with sNMF provided a picture of genetic patterns across the TSI for
381 $K = 2$ (Fig 1). Despite the higher resolution of SNP markers and the additional ~3-11 years
382 elapsed since sampling, there was no clearer spatial genetic structure within and between
383 villages at $K = 2$ than in the previous microsatellite study (c.f. Maynard et al., 2017). Both
384 ancestral lineages were detected in every village, though 48 individuals were assessed as not
385 admixed (Fig 1). Genetic admixture among individuals was highly variable in some villages,
386 particularly in D:Badu, G:Warraber, I:Masig and L:Mer. Despite this, some geographical patterns
387 were evident from the $K = 2$ analysis, particularly the genetic similarity of the central islands
388 (F:Iama, G:Warraber, H:Poruma) and those of Moa Island (B:St Pauls and C:Kubin). These
389 patterns are increasingly pronounced at $K = 3$ (Figure S16), though the high admixture within
390 villages (Figures 1, S15, S16, S17) and low pairwise F_{ST} among villages (Table S2) indicate that
391 genetic structure is weak within the TSI. Genetic similarity among the central islands has
392 previously been noted (Maynard et al., 2017), and points to temporal consistency in genetic
393 structure.

394 Mean global F_{ST} among villages in 2018 was 0.039 (SE = 0.000) while differentiation (D_{est}) was
395 0.006 (SE = 0.000). Pairwise F_{ST} estimates between villages (Table S2) indicate that I:Masig had
396 higher average pairwise F_{ST} in 2019 ($\bar{x} = 0.032$, SE = 0.001) than in 2018 ($\bar{x} = 0.029$, SE = 0.001),
397 an average increase in F_{ST} of 8.9% over the 12 months, perhaps reflecting the development of
398 additional genetic structure across time. Tajima's D can be difficult to interpret, but the

399 consistently negative mean values across all villages accord with past population expansions
400 following colonisation (Gattepaille, Jakobsson, & Blum, 2013).

401

402 ***Dispersal within villages***

403 Table 1 lists mean pairwise genetic distance (Rousset's a) for dyads sampled at < 50 m and > 500
404 m separation within each village. Mosquitoes sampled at > 500 m separation did not have
405 consistently higher genetic distances than those sampled at < 50 m separation. Likewise, 6 of
406 the 13 Mantel tests showed a negative relationship between genetic and geographic distance
407 within villages (Figures S18-S30). There was no statistically significant isolation by distance
408 within any of the villages (all Bonferroni-corrected P-values > 0.05).

409 When within-village dyads were concatenated to estimate neighbourhood size (N_w), isolation by
410 distance was revealed by the positive relationship between genetic distance (Rousset's a) and
411 the natural logarithm of geographical distance (geodist): $a = 0.003025 \times \text{geodist} + 0.1878$, with
412 coefficient SE = 0.00129. N_w within villages was estimated at $\frac{1}{0.003025} = 331$ mosquitoes (95%
413 C.I. 232–577). Despite high variability among villages, these results indicate that TSI *Ae.*
414 *albopictus* have some spatial structure at scales of 100s to 1000s of metres.

415

416 ***Close kin within villages***

417 Three of the 2772 dyads within villages had putative first-order relatedness, and none had
418 second-order relatedness (Table 2). Two of the three dyads were collected at the same sampling
419 point, the other at points 170 m apart. This low incidence of close kin compared with other
420 studies (e.g. Jasper et al., 2019) was likely due to the 100 m separation between most sampling
421 points and suggests mostly local movement within villages.

422

423 ***Close kin across villages***

424 Within villages, the dyad in E:Mabuiag had the lowest PC-Relate kinship coefficient of the three
425 close kin dyads (0.32 with 3 PCs; Table 2), so this was used as the cut-off for designating close
426 kin across villages. Five of the 31,944 dyads across villages had higher scores than this,
427 indicating putative first-order relatedness. The three highest kinship coefficients for 'unrelated'
428 dyads were 0.27, 0.23, and 0.16. When 5 or 10 PCs were included, the rank order of kinship
429 coefficients fluctuated but all remained consistently above the within-village cut-off and above
430 the coefficients of unrelated dyads.

431 Four of the putative close kin dyads were across nearby villages while the fifth was between
432 E:Mabuiag and L:Mer, ~200 km apart (Figure 1, Table 2). For each dyad the direction of dispersal
433 was apparent, demonstrated by both individuals in the dyad having higher mean kinship
434 coefficients with Village-2 (the origin) than Village-1 (the destination). Results of t-tests
435 assessing dispersal direction were all strongly statistically significant (all $t > 8.6$, all $P < 0.001$).

436

437

438

439 ***Incursions past the *cordon sanitaire****

440 The two methods of assignment, assignPOP and Locator, provided concordant results for two of
441 the incursives (Fig 2). Inc-1 and Inc-2 had both clearly dispersed from A:Keriri, less than 10 km
442 from where they were detected on Ngurapai (Fig 2: x). In assignPOP this was demonstrated by
443 the high posterior (0.90 and 0.77) and relative (61.3 and 16.8) probabilities of assignment to
444 A:Keriri. For Locator each incursive was placed among the A:Keriri genotypes for the clear

445 majority of the 1000 bootstrap subsamples (Fig 2). Point estimates from Locator placed Inc-1
446 (10.5562° S, 142.2197° E) and Inc-2 (10.5585° S, 142.2173° E) amidst the A:Keriri samples.

447 Inc-3 and Inc-4 were assigned differently by assignPOP and Locator. This was not likely due to
448 missing data (3.8% and 8.3%), as successful assignments with assignPOP have been recorded
449 with > 40% missing data (Schmidt et al., 2019). assignPOP selected distant L:Mer (Inc-3) and
450 I:Masig (Inc-4) as the most likely sources, though posterior (0.35 and 0.16) and relative (2.8 and
451 1.1) probabilities were low. Locator point estimates placed Inc-3 (10.2086° S, 142.2910° E) on
452 Moa Island between the B:St Pauls and C:Kubin genotypes. Inc-4 (9.9216° S, 143.1598° E) was
453 placed in the Torres Strait near I:Masig. Bootstrap subsampling revealed higher uncertainty for
454 Inc-3 than for Inc-1 and Inc-2 but nevertheless indicated Moa Island was the likely source. No
455 clear assignment was forthcoming for Inc-4.

456

457

458 International gene flow into the Torres Strait

459 ***Genome-wide gene flow***

460 The *fineRADstructure* plot (Fig 3) shows coancestry between genotype pairs from TSI and other
461 selected locations. See Figure S31 for the figure at full size, and Figure S32 for a PCA-UMAP
462 ordination of the same genotypes using the same colour symbology. TSI genotypes were only
463 weakly clustered by location, as seen by the poor 'sorting' of genotypes in the colour panel.
464 Only one village (J:Ugar) had every genotype resolved into a single lineage. However, TSI
465 genotypes formed a lineage with Indonesia and Timor-Leste (Fig 3: solid black square, top right)
466 distinct from all other genotypes (solid black square, bottom left).

467 Within these broad groups were subgroups (Fig 3: dashed squares) placing East and Southeast
468 Asian genotypes together with Fiji and Indonesian genotypes with Timor-Leste, as expected
469 from previous analysis (Schmidt, Chung, Honnen, et al., 2020; Schmidt, Chung, van Rooyen, et

470 al., 2020). PNG genotypes grouped with Vanuatu, suggesting recent coancestry. While the PNG
471 and Vanuatu lineage had slightly greater coancestry with Southeast Asia than East Asia, this
472 lineage was clearly differentiated from all others. PCA-UMAP confirmed the three major groups
473 of TSI/Indonesia/Timor-Leste, East Asia/Southeast Asia/Fiji, and PNG/Vanuatu (Figure S32).

474 Gene flow from PNG into the TSI was suggested by the higher coancestry between PNG and
475 some TSI genotypes, particularly those from L:Mer (Fig 3: blue asterisks). PNG also had higher
476 coancestry with Jakarta and Bandung in Indonesia but not with Bali. While there was some
477 evidence of coancestry between East Asian and TSI genotypes, this was also observed in East
478 Asian and Indonesian genotypes, particularly those from Jakarta and Bandung. It was thus
479 unclear whether recent gene flow had occurred from East Asia into the TSI or whether past
480 gene flow from East Asia into Indonesia had introduced alleles that were then brought to the TSI
481 during invasion.

482 Table 1 lists the number of private alleles in each village with and without the PNG samples
483 included in filtering. When PNG was included, the greatest 'loss' of private alleles was observed
484 in the eastern islands of I:Masig (30% loss), J:Ugar (35% loss), K:Erub (32% loss), and L:Mer (48%
485 loss) and northern island of F:lama (29% loss). These 'lost' alleles are identical by state and likely
486 also identical by descent to those in PNG, indicating gene flow between each island and PNG.
487 Notably, the fact that these alleles were not found on other islands suggests that this gene flow
488 was also specific to each island, and thus is not due to one single incursion into the TSI followed
489 by local spread.

490

491 ***Adaptive introgression***

492 Outlier analysis revealed four genomic regions of interest, each containing irregularly structured
493 SNPs spread across multiple RADtags within 1 Mbp, and detected as outliers by both *pcadapt*
494 and sNMF. For *pcadapt*, a scree plot of the proportion of explained variance did not indicate an

495 optimum K (Figure S33). However, visual inspection of scatterplots of the first eight PCs
496 indicated that genetic structure among villages was much less apparent after the first four PCs
497 (Figures S34-37). Accordingly, we restricted our analyses to $2 \leq K \leq 4$ for both programs.

498 The four genomic regions and all genes of known function contained therein are listed in Tables
499 S3-S6. One of these regions, consisting of four SNPs across two RADtags ~330 kbp apart on
500 scaffold NW_021838465.1, contained 12 genes of interest (Table S3). These included three
501 cytochrome P450 9e2-like genes and nine probable cytochrome P450 9f2 genes. Cytochrome
502 P450 9e2 genes have been linked to insecticide resistance and demonstrated strong
503 upregulation in resistant *Ae. aegypti* mosquitoes (Kim Lien et al., 2019). Cytochrome P450 9f2
504 genes have also been linked to insecticide resistance (Etebari et al., 2018). The four SNPs
505 enclosing the region were detected as outliers for all $2 \leq K \leq 4$ settings and were detected in
506 both the imputed and unimputed datasets, which likely reflects the low missing data ($\bar{x} = 5.1\%$)
507 at these SNPs.

508 We investigated these four SNPs more closely using the unimputed dataset from the entire
509 Indo-Pacific region (Table 3). Non-reference alleles at these SNPs were found most frequently as
510 a single linked haplotype, which in the TSI was detected at highest frequency on I:Masig (2018
511 and 2019) but also on A:Keriri and L:Mer. Outside of the TSI this haplotype was found only in
512 Port Moresby in PNG. Considering non-reference alleles at the four SNPs individually, outside of
513 the TSI and Port Moresby the only observation was a single individual from Singapore, which
514 had two alleles identical by state at one of the SNPs (Table 3). Tables S7 and S8 list unimputed
515 genotypes at these SNPs for all TSI individuals (Table S7) and all non-TSI individuals (Table S8).
516 These show clear but imperfect patterns of linkage between the two RADtags, and clear
517 geographical restrictions in where the alleles were found.

518

519

520 Discussion

521

522 Spatial population genomics provides a powerful framework for investigating recent invasions.
523 Our spatially consistent sampling within villages and simultaneous sampling across islands has
524 permitted a range of analyses appropriate for characterising dispersal and adaptation in the
525 recent *Ae. albopictus* invasion of the Torres Strait. Our findings point to a highly interconnected
526 invasive metapopulation with frequent dispersal among both adjacent and non-adjacent
527 islands, including incursions into uninvaded islands below the *cordon sanitaire*. The connectivity
528 of this system also extends beyond borders, with evidence of gene flow from PNG into several
529 of the nearest islands. Some of this gene flow was strongly suggestive of adaptive introgression,
530 specifically at a set of linked outlier SNPs surrounding a genomic region containing 12
531 cytochrome P450 genes, of types (9e2 and 9f2) previously associated with insecticide resistance
532 (Etebari et al., 2018; Kim Lien et al., 2019). Non-reference alleles at these outlier SNPs were
533 found in four TSI villages, but not in any of the Indonesian populations from which the original
534 invasion was sourced, or any population other than Port Moresby (PNG south coast), indicating
535 a potential cross-country ‘genetic invasion’ of resistance alleles introgressed from southern PNG
536 to the TSI. Broad-scale patterns of passive dispersal across islands contrasted with fine-scale
537 patterns of active dispersal within villages, where spatial genetic structure was locally variable
538 but displayed general trends of isolation by distance and neighbourhood size (N_W : Wright, 1946)
539 of 232–577.

540 When geographical genetic structure is weak, as in the TSI (Fig 1, Fig 3), this is often read as a
541 sign of high gene flow between subregions (Bossart & Prowell, 1998). However, in new
542 invasions this conclusion can be confounded by high regional coancestry stemming from the
543 original invasion (Cristescu, 2015; Fitzpatrick et al., 2012). This study instead investigated
544 dispersal by analysing close kin dyads, incursions below the *cordon sanitaire*, and gene flow
545 from PNG. Kinship and incursion tracing both reveal dispersal patterns over the past ~1-2

546 generations, and these methods should not be confounded by regional coancestry as they were
547 either calibrated against estimates from within villages (kinship) or traced incursive mosquitoes
548 to anywhere in continuous space within the region (incursions: Locator). Of the four incursives,
549 only Inc-4 was likely confounded by coancestry, as seen by its central placement among the
550 training genotypes (Fig 2). Likewise, international gene flow had no trouble with coancestry as
551 the source of gene flow (PNG) was genetically very distinct from the source of the initial
552 invasion (Indonesia) (Fig 3, Figure S32). Together these analyses suggest that long-distance
553 dispersal is frequent throughout the region, though movement between nearby islands may be
554 more common than between distant islands (Fig 2, Table 2). Despite evidence of direct gene
555 flow from PNG (Table 1), the TSI retains a distinct genetic background (Fig 3), indicating that if
556 any local eradication has occurred as postulated in Muzari et al. (2017) these islands would have
557 been recolonised primarily from within the TSI. The consistent clustering of PNG and Vanuatu
558 genotypes indicate the Vanuatuan *Ae. albopictus* invasion was likely established from PNG or
559 another location of that lineage like the Solomon Islands (see Maynard et al., 2017).

560 These patterns of variation are similar to those found in some biological invasions but contrast
561 with others where variation reflects ongoing founder events as a colonising species spreads.
562 Similar patterns to those observed here have been established for western flower thrips where
563 high rates of ongoing gene flow mediated by human transport have been hypothesised (Cao et
564 al., 2017). In contrast, regional genetic patterns reflective of repeated colonisations with small
565 sample sizes have been documented in other thrips where distant colonisation into vacant
566 habitat is likely to have occurred (Cao et al., 2019), as well as where there have been intensive
567 campaigns with chemical insecticides to subdue populations (Cao et al., 2017). For TSI *Ae.*
568 *albopictus*, it appears that human-mediated migration has had a stronger effect on population
569 structure than control efforts aiming to suppress populations. In this sense, the TSI *Ae.*
570 *albopictus* appear to be structured as a metapopulation similar to classical metapopulations like
571 Glanville fritillary butterflies (Fountain et al., 2018; Hanski et al., 2017).

572 Although movement between islands has been suggested in previous studies (Beebe et al.,
573 2013; Maynard et al., 2017), this study provides the first evidence of dispersal between specific
574 islands. Our kinship analysis builds on previous uses of close kin to detect recent dispersal (M. Z.
575 Chen et al., 2020; Escoda et al., 2019, 2017; Fountain et al., 2018; Jasper et al., 2019; Schmidt et
576 al., 2018, 2017; Trense et al., 2020), and here demonstrates the use of regional genetic distance
577 patterns to also infer the direction of movement (Fig 1, Table 2). Inferring movement patterns
578 across single generations in this manner is becoming increasingly popular in applied work on
579 pests and conservation, where recent changes in demography and genetic structure mean that
580 assumptions of equilibrium demography are invalid and where anthropogenic impacts are
581 observed from one generation to the next. First order kin detected across islands were likely
582 transported via aeroplane, barge or small vessel movement. Although aircraft disinsection
583 (treatment with insecticides) is currently compulsory for all air travel between the TSI region
584 and the mainland of Australia, flights among the islands are not always disinfected. Future
585 research could investigate the relative contributions of different transport networks to *Ae.*
586 *albopictus* dispersal between islands and into the TSI from PNG.

587 The power of higher-resolution markers to better delineate geographical patterns among
588 genotypes is well-established (Escoda et al., 2017; Puckett & Eggert, 2016; Rašić et al., 2014).
589 While previous investigation of this system with lower-resolution markers detected some spatial
590 structuring among islands (Maynard et al., 2017), this study found no greater sorting of
591 genotypes by location despite higher marker power and despite sampling in this study having
592 taken place 3-11 years later (Fig 1, Fig 3). These results point to the TSI *Ae. albopictus*
593 population remaining highly interconnected over time. This interconnection is likely the reason
594 for high genetic variability within villages, including the inconsistent spatial structuring of
595 genetic variation among dyads (Table 1). Nevertheless, our estimate of N_w in villages (232 –
596 577) is consistent with a previous estimate for an urban *Ae. aegypti* population (268; Jasper et
597 al., 2019). Considering high densities of *Ae. albopictus* in the TSI, this estimate of N_w is
598 suggestive of some spatial structure within villages.

599 Despite high regional gene flow, we managed to locate the source of 2-3 of the 4 incursions
600 below the *cordon sanitaire*. Considering the absence of discrete populations within the TSI, the
601 genotype-based method of Locator (Battey et al., 2020) was better suited to this dataset than
602 the allele-frequency based method of assignPOP (K.-Y. Chen et al., 2018), though the latter still
603 performed well for Inc-1 and Inc-2 and both methods successfully traced samples collected 10
604 months after the initial collections. Although Locator may best be suited to non-clustered
605 sampling designs that are rare in island systems, Locator may sidestep issues relating to invasion
606 age and frequent gene flow by not requiring that reference genotypes be sorted into
607 populations. Locator's placement of Inc-4 across a wide swathe of the sampling range (Fig 2)
608 indicated that this sample could not be assigned, which was not likely due to missing data but
609 due to recent ancestry from multiple locations. If we treat the placement of Inc-4 as the
610 expected outcome of a failure to assign, then the placement of Inc-3 on Moa Island with closely-
611 clustered bootstrap replicates suggests that this is its likely origin. While population assignment
612 methods such as assignPOP perform well when determining incursion sources pre-invasion
613 (Schmidt, Chung, van Rooyen, et al., 2020; Schmidt et al., 2019), Locator appears a more useful
614 tool for tracing local incursions after an initial invasion.

615 Detecting adaptive introgression is a powerful application of genomic datasets. For invasive
616 systems adaptive introgression can be classed as a type of genetic invasion, in which alleles
617 conferring a selective advantage that may interfere with control strategies are introduced after
618 an initial invasion (Endersby-Harshman et al., 2020; Riveron et al., 2013; Schmidt et al., 2019).
619 Our detection of a set of alleles from PNG that have introgressed into the TSI is strongly
620 suggestive of a genetic invasion. In the TSI, introgressed alleles at the four outlier SNPs were
621 found on four of the islands, but were particularly common on I:Masig, where their frequency
622 remained stable between 2018 and 2019. Considering the current low allele frequencies on
623 most of the islands, the imperfect linkage between the alleles, and the abandonment of the
624 insecticide program in the TSI a decade previously (Muzari et al., 2017), our observations may
625 reflect the aftermath of a genetic invasion that spread into the TSI during the height of the
626 insecticide program. During this time, I:Masig may have been acting as an 'invasive bridgehead'

627 (Estoup & Guillemaud, 2010) for the genetic invasion, from which resistance alleles spread to
628 other islands.

629 While traditionally 'introgression' refers to the interspecific transfer of genetic material, which
630 has also been observed in mosquitoes (Norris et al., 2015), introgression between differentiated
631 populations as observed here may be more common and may allow for faster spread of
632 advantageous alleles if interspecific mating is rare or confers greater fitness costs. Considering
633 also the connectivity of the TSI/PNG system, where dispersal takes place among distant islands
634 and across countries, if advantageous alleles arise in any given location they may rapidly spread
635 throughout the region if similar selective pressures are present. This rapid spread of alleles may
636 be a threat in any biological system with high dispersal rates and common selective pressures.
637 In the TSI, linkage was strong between the two RADtags surrounding the 12 cytochrome P450
638 genes, though not as strong as the near-perfect linkage observed around pyrethroid resistance
639 mutations in *Ae. aegypti* (Endersby-Harshman et al., 2020). This may reflect relatively weaker
640 selection around the cytochrome P450 genes given that area-wide insecticide use in the TSI was
641 phased out ~10 years before sampling for this project (Muzari et al., 2017) and that in PNG most
642 documented insecticide use occurs outside of cities like Port Moresby (Demok et al., 2019).
643 While recent bioassays on PNG *Ae. albopictus* demonstrated resistance to DDT, these
644 investigated only Madang *Ae. albopictus* (Demok et al., 2019), though emerging results indicate
645 these resistance patterns are similar across PNG (unpublished data). Nevertheless, the detected
646 introgression was evidently not from Madang but from either Port Moresby or an unsampled
647 location in PNG. Future work is needed to determine what role the 12 cytochrome P450 genes
648 have in conferring insecticide resistance in this system and in *Ae. albopictus* more broadly.

649

650

651 **Conclusions**

652 Dispersal can be difficult to investigate in many biological systems, particularly those subjected
653 to different ongoing dispersal processes. The recent biological invasion of *Ae. albopictus* into TSI
654 provides an example of such a system, and here we have performed a comprehensive
655 characterisation of dispersal using temporally-restricted sampling and an appropriate set of
656 population genomic analyses. We detected recent dispersal between distant and adjacent
657 islands and found no increase in spatial genetic structure over time, suggesting that the invaded
658 islands may best be considered a metapopulation connected by frequent gene flow, rather than
659 individual 'populations'. We also made use of the strongly-differentiated PNG *Ae. albopictus*
660 population to detect gene flow from PNG into specific islands, and found evidence that a
661 genetic invasion of insecticide resistance alleles may have spread into the TSI from the south
662 coast of PNG. These methods will be broadly applicable to other taxa, particularly those affected
663 by anthropogenic processes. For *Ae. albopictus*, the findings inform strategies for the control of
664 this globally-invasive pest across a broad range of spatial scales.

665

666 **Acknowledgements**

667 For sample collection we thank Esther Anderson, Moses Laman, Rotarians against Malaria PNG
668 staff, and the PNGIMR Vector Borne Disease Unit entomology team. We thank Moshe Jasper for
669 helpful discussions. For funding we thank Queensland Health, the Commonwealth Department
670 of Health, the Far North Queensland Hospital Foundation (FNQHF), and the NHMRC
671 (Programme Grant 1037003, Career Development Fellowship 1141441, and Fellowship Grants
672 1118640 and 5121190). T.S. was financially supported by a Australian Government Research
673 Training Program Scholarship.

674

675 **Data Accessibility**

676 Aligned .bam sequence files for 331 TSI *Ae. albopictus*, 4 incursive *Ae. albopictus*, and 36 PNG
677 *Ae. albopictus* are available through the Sequence Read Archive at NCBI Genbank:
678 PRJNA684450.

679

680 Author Contributions

681 TLS, TS, GE, SR, and AAH designed the study. TS, SK, SD, QY, MOM, GE, MB, RB and PH collected
682 the data. TLS, TS, JC and MAF analysed the data. TLS, MAF, GE, TRB, SR and AAH provided
683 supervision. TLS, TS and AAH wrote the paper with edits from all authors.

684 References

685

686 Battey, C. J., Ralph, P. L., & Kern, A. D. (2020). Predicting geographic location from genetic variation with
687 deep neural networks. *ELife*, 9, 1–22. doi: 10.7554/eLife.54507

688 Beebe, N. W., Ambrose, L., Hill, L. A., Davis, J. B., Hapgood, G., Cooper, R. D., ... van den Hurk, A. F.

689 (2013). Tracing the Tiger: Population Genetics Provides Valuable Insights into the *Aedes*
690 (*Stegomyia*) *albopictus* Invasion of the Australasian Region. *PLoS Neglected Tropical Diseases*, 7(8),
691 e2361. doi: 10.1371/journal.pntd.0002361

692 Bossart, J. L., & Prowell, D. P. (1998). Genetic estimates of population structure and gene flow:

693 Limitations, lessons and new directions. *Trends in Ecology and Evolution*, 13(5), 202–206. doi:
694 10.1016/S0169-5347(97)01284-6

695 Bradburd, G. S., & Ralph, P. L. (2019). Spatial Population Genetics: It's about Time. *Annual Review of*

696 *Ecology, Evolution, and Systematics*, 50(1), 427–449. doi: 10.1146/annurev-ecolsys-110316-022659

697 Browning, B. L., & Browning, S. R. (2016). Genotype Imputation with Millions of Reference Samples. *The*

698 *American Journal of Human Genetics*, 98(1), 116–126. doi: 10.1016/J.AJHG.2015.11.020

699 Cao, L., Gao, Y., Gong, Y., Chen, J., Chen, M., Hoffmann, A., & Wei, S. (2019). Population analysis reveals

700 genetic structure of an invasive agricultural thrips pest related to invasion of greenhouses and
701 suitable climatic space. *Evolutionary Applications*, 12(10), 1868–1880. doi: 10.1111/eva.12847

702 Cao, L. J., Wang, Z. H., Gong, Y. J., Zhu, L., Hoffmann, A. A., & Wei, S. J. (2017). Low genetic diversity but
703 strong population structure reflects multiple introductions of western flower thrips (Thysanoptera:
704 Thripidae) into China followed by human-mediated spread. *Evolutionary Applications*, 10(4), 391–
705 401. doi: 10.1111/eva.12461

706 Catchen, J., Hohenlohe, P. A., Bassham, S., Amores, A., & Cresko, W. A. (2013). Stacks: an analysis tool set
707 for population genomics. *Molecular Ecology*, 22(11), 3124–3140. doi: 10.1111/mec.12354

708 Chen, K.-Y., Marschall, E. A., Sovic, M. G., Fries, A. C., Gibbs, H. L., & Ludsin, S. A. (2018). *assignPOP*: An R
709 package for population assignment using genetic, non-genetic, or integrated data in a machine-
710 learning framework. *Methods in Ecology and Evolution*, 9(2), 439–446. doi: 10.1111/2041-
711 210X.12897

712 Chen, M. Z., Cao, L. J., Li, B. Y., Chen, J. C., Gong, Y. J., Yang, Q., ... Wei, S. J. (2020). Migration trajectories
713 of the diamondback moth *Plutella xylostella* in China inferred from population genomic variation.
714 *Pest Management Science*, ps.6188. doi: 10.1002/ps.6188

715 Combs, M., Puckett, E. E., Richardson, J., Mims, D., & Munshi-South, J. (2018). Spatial population
716 genomics of the brown rat (*Rattus norvegicus*) in New York City. *Molecular Ecology*, 27(1), 83–98.
717 doi: 10.1111/mec.14437

718 Conomos, M. P., Reiner, A. P., Weir, B. S., & Thornton, T. A. (2016). Model-free Estimation of Recent
719 Genetic Relatedness. *American Journal of Human Genetics*, 98(1), 127–148. doi:
720 10.1016/j.ajhg.2015.11.022

721 Cristescu, M. E. (2015). Genetic reconstructions of invasion history. *Molecular Ecology*, 24(9), 2212–
722 2225. doi: 10.1111/mec.13117

723 Danecek, P., Auton, A., Abecasis, G., Albers, C. A., Banks, E., DePristo, M. A., ... Durbin, R. (2011). The
724 variant call format and VCFtools. *Bioinformatics*, 27(15), 2156–2158. doi:
725 10.1093/bioinformatics/btr330

726 Demok, S., Endersby-Harshman, N., Vinit, R., Timinao, L., Robinson, L. J., Susapu, M., ... Karl, S. (2019).

- 727 Insecticide resistance status of *Aedes aegypti* and *Aedes albopictus* mosquitoes in Papua New
728 Guinea. *Parasites and Vectors*, 12(1), 333. doi: 10.1186/s13071-019-3585-6
- 729 Diaz-Papkovich, A., Anderson-Trocmé, L., Ben-Eghan, C., & Gravel, S. (2019). UMAP reveals cryptic
730 population structure and phenotype heterogeneity in large genomic cohorts. *PLoS Genetics*, 15(11).
731 doi: 10.1371/journal.pgen.1008432
- 732 Dray, S., & Dufour, A. B. (2007). The ade4 package: Implementing the duality diagram for ecologists.
733 *Journal of Statistical Software*, 22(4), 1–20. doi: 10.18637/jss.v022.i04
- 734 Endersby-Harshman, N. M., Schmidt, T. L., Chung, J., van Rooyen, A., Weeks, A. R., & Hoffmann, A. A.
735 (2020). Heterogeneous genetic invasions of three insecticide resistance mutations in Indo-Pacific
736 populations of *Aedes aegypti* (L.). *Molecular Ecology*, 29(9), 1628–1641. doi: 10.1111/mec.15430
- 737 Escoda, L., Fernández-González, Á., & Castresana, J. (2019). Quantitative analysis of connectivity in
738 populations of a semi-aquatic mammal using kinship categories and network assortativity.
739 *Molecular Ecology Resources*, 19(2), 310–326. doi: 10.1111/1755-0998.12967
- 740 Escoda, L., González-Esteban, J., Gómez, A., & Castresana, J. (2017). Using relatedness networks to infer
741 contemporary dispersal: Application to the endangered mammal *Galemys pyrenaicus*. *Molecular*
742 *Ecology*, 26(13), 3343–3357. doi: 10.1111/mec.14133
- 743 Estoup, A., & Guillemaud, T. (2010). Reconstructing routes of invasion using genetic data: Why, how and
744 so what? *Molecular Ecology*, 19(19), 4113–4130. doi: 10.1111/j.1365-294X.2010.04773.x
- 745 Etebari, K., Afrad, M. H., Tang, B., Silva, R., Furlong, M. J., & Asgari, S. (2018). Involvement of microRNA
746 miR-2b-3p in regulation of metabolic resistance to insecticides in *Plutella xylostella*. *Insect*
747 *Molecular Biology*, 27(4), 478–491. doi: 10.1111/imb.12387
- 748 Fitzpatrick, B. M., Fordyce, J. A., Niemiller, M. L., & Reynolds, R. G. (2012). What can DNA tell us about
749 biological invasions? *Biological Invasions*, 14(2), 245–253. doi: 10.1007/s10530-011-0064-1
- 750 Fitzpatrick, B. M., Johnson, J. R., Kump, D. K., Smith, J. J., Voss, S. R., & Shaffer, H. B. (2010). Rapid spread
751 of invasive genes into a threatened native species. *Proceedings of the National Academy of Sciences*
752 *of the United States of America*, 107(8), 3606–3610. doi: 10.1073/pnas.0911802107
- 753 Fountain, T., Husby, A., Nonaka, E., DiLeo, M. F., Korhonen, J. H., Rastas, P., ... Hanski, I. (2018). Inferring

- 754 dispersal across a fragmented landscape using reconstructed families in the Glanville fritillary
755 butterfly. *Evolutionary Applications*, 11(3), 287–297. doi: 10.1111/eva.12552
- 756 Frichot, E., & François, O. (2015). LEA : An R package for landscape and ecological association studies.
757 *Methods in Ecology and Evolution*, 6(8), 925–929. doi: 10.1111/2041-210X.12382
- 758 Gattepaille, L. M., Jakobsson, M., & Blum, M. G. B. (2013, May 20). Inferring population size changes with
759 sequence and SNP data: Lessons from human bottlenecks. *Heredity*, Vol. 110, pp. 409–419. Nature
760 Publishing Group. doi: 10.1038/hdy.2012.120
- 761 Gillespie, R. G., Baldwin, B. G., Waters, J. M., Fraser, C. I., Nikula, R., & Roderick, G. K. (2012). Long-
762 distance dispersal: a framework for hypothesis testing. *Trends in Ecology and Evolution*, 27(1), 47–
763 56. doi: 10.1016/j.tree.2011.08.009
- 764 Goubert, C., Henri, H., Minard, G., Valiente Moro, C., Mavingui, P., Vieira, C., & Boulesteix, M. (2017).
765 High-throughput sequencing of transposable element insertions suggests adaptive evolution of the
766 invasive Asian tiger mosquito towards temperate environments. *Molecular Ecology*, 26(15), 3968–
767 3981. doi: 10.1111/mec.14184
- 768 Goudet, J. (2005). HIERFSTAT, a package for R to compute and test hierarchical F-statistics. *Molecular*
769 *Ecology Notes*, 5(1), 184–186. doi: 10.1111/j.1471-8286.2004.00828.x
- 770 Hanski, I., Schulz, T., Wong, S. C., Ahola, V., Ruokolainen, A., & Ojanen, S. P. (2017). Ecological and
771 genetic basis of metapopulation persistence of the Glanville fritillary butterfly in fragmented
772 landscapes. *Nature Communications*, 8(1), 1–11. doi: 10.1038/ncomms14504
- 773 Hardy, O. J., & Vekemans, X. (2002). SPAGeDi: a versatile computer program to analyse spatial genetic
774 structure at the individual or population levels. *Molecular Ecology Notes*, 2(4), 618–620. doi:
775 10.1046/j.1471-8286.2002.00305.x
- 776 Harrington, L. C., Scott, T. W., Lerdthusnee, K., Coleman, R. C., Costero, A., Clark, G. G., ... Edman, J. D.
777 (2005). Dispersal of the dengue vector *Aedes aegypti* within and between rural communities. *The*
778 *American Journal of Tropical Medicine and Hygiene*, 72(2), 209–220. doi:
779 10.4269/ajtmh.2005.72.209
- 780 Hengeveld, R. (1989). *Dynamics of biological invasions*. London: Chapman & Hall.

- 781 Hoban, S., Kelley, J. L., Lotterhos, K. E., Antolin, M. F., Bradburd, G., Lowry, D. B., ... Whitlock, M. C.
782 (2016). Finding the genomic basis of local adaptation: Pitfalls, practical solutions, and future
783 directions. *American Naturalist*, 188(4), 379–397. doi: 10.1086/688018
- 784 Howard, W. E. (1960). Innate and Environmental Dispersal of Individual Vertebrates. *American Midland*
785 *Naturalist*, 63(1), 152–161. doi: 10.2307/2422936
- 786 Jasper, M., Schmidt, T. L., Ahmad, N. W., Sinkins, S. P., & Hoffmann, A. A. (2019). A genomic approach to
787 inferring kinship reveals limited intergenerational dispersal in the yellow fever mosquito. *Molecular*
788 *Ecology Resources*, 19(5), 1254–1264. doi: 10.1111/1755-0998.13043
- 789 Johansen, C. A., Van Den Hurk, A. F., Ritchie, S. A., Zborowski, P., Nisbet, D. J., Paru, R., ... Mackenzie, J. S.
790 (2000). Isolation of Japanese encephalitis virus from mosquitoes (Diptera: Culicidae) collected in
791 the western province of Papua New Guinea, 1997-1998. *American Journal of Tropical Medicine and*
792 *Hygiene*, 62(5), 631–638. doi: 10.4269/ajtmh.2000.62.631
- 793 Jost, L. (2008). GST and its relatives do not measure differentiation. *Molecular Ecology*, 17(18), 4015–
794 4026. doi: 10.1111/j.1365-294X.2008.03887.x
- 795 Kim Lien, N. T., Hong Ngoc, N. T., Lan, N. N., Hien, N. T., Van Tung, N., Thanh Ngan, N. T., ... Huong Binh,
796 N. T. (2019). Transcriptome Sequencing and Analysis of Changes Associated with Insecticide
797 Resistance in the Dengue Mosquito (*Aedes aegypti*) in Vietnam. *American Journal of Tropical*
798 *Medicine and Hygiene*, 100(5), 1240–1248. doi: 10.4269/ajtmh.18-0607
- 799 Langmead, B., & Salzberg, S. L. (2012). Fast gapped-read alignment with Bowtie 2. *Nature Methods*, 9(4),
800 357–359. doi: 10.1038/nmeth.1923
- 801 Linck, E., & Battey, C. J. (2019). Minor allele frequency thresholds strongly affect population structure
802 inference with genomic data sets. *Molecular Ecology Resources*, 19(3), 639–647. doi: 10.1111/1755-
803 0998.12995
- 804 Luu, K., Bazin, E., & Blum, M. G. B. (2017). pcadapt : an R package to perform genome scans for selection
805 based on principal component analysis. *Molecular Ecology Resources*, 17(1), 67–77. doi:
806 10.1111/1755-0998.12592
- 807 Malinsky, M., Trucchi, E., Lawson, D. J., & Falush, D. (2018). RADpainter and fineRADstructure:

808 Population Inference from RADseq Data. *Molecular Biology and Evolution*, 35(5), 1284–1290. doi:
809 10.1093/molbev/msy023

810 Manichaikul, A., Mychaleckyj, J. C., Rich, S. S., Daly, K., Sale, M., & Chen, W. M. (2010). Robust
811 relationship inference in genome-wide association studies. *Bioinformatics*, 26(22), 2867–2873. doi:
812 10.1093/bioinformatics/btq559

813 Maynard, A. J., Ambrose, L., Cooper, R. D., Chow, W. K., Davis, J. B., Muzari, M. O., ... Beebe, N. W.
814 (2017). Tiger on the prowl: Invasion history and spatio-temporal genetic structure of the Asian tiger
815 mosquito *Aedes albopictus* (Skuse 1894) in the Indo-Pacific. *PLOS Neglected Tropical Diseases*,
816 11(4), e0005546. doi: 10.1371/journal.pntd.0005546

817 Mcfarlane, J. (1998). Torres Strait: Policing the Open Border. *Trends and Issues in Crime and Criminal*
818 *Justice*, 1–6. Canberra: Australian Institute of Criminology. Retrieved from <http://www.aic.gov.au>

819 Muzari, M. O., Devine, G., Davis, J., Crunkhorn, B., van den Hurk, A., Whelan, P., ... Ritchie, S. (2017).
820 Holding back the tiger: Successful control program protects Australia from *Aedes albopictus*
821 expansion. *PLOS Neglected Tropical Diseases*, 11(2), e0005286. doi: 10.1371/journal.pntd.0005286

822 Norris, L. C., Main, B. J., Lee, Y., Collier, T. C., Fofana, A., Cornel, A. J., & Lanzaro, G. C. (2015). Adaptive
823 introgression in an African malaria mosquito coincident with the increased usage of insecticide-
824 treated bed nets. *Proceedings of the National Academy of Sciences of the United States of America*,
825 112(3), 815–820. doi: 10.1073/pnas.1418892112

826 Palatini, U., Masri, R. A., Cosme, L. V., Koren, S., Thibaud-Nissen, F., Biedler, J. K., ... Bonizzoni, M. (2020).
827 Improved reference genome of the arboviral vector *Aedes albopictus*. *BioRxiv*, 2020.02.28.969527.
828 doi: 10.1101/2020.02.28.969527

829 Pélessié, B., Crossley, M. S., Cohen, Z. P., & Schoville, S. D. (2018, April 1). Rapid evolution in insect pests:
830 the importance of space and time in population genomics studies. *Current Opinion in Insect Science*,
831 Vol. 26, pp. 8–16. Elsevier Inc. doi: 10.1016/j.cois.2017.12.008

832 Puckett, E. E., & Eggert, L. S. (2016). Comparison of SNP and microsatellite genotyping panels for spatial
833 assignment of individuals to natal range: A case study using the American black bear (*Ursus*
834 *americanus*). *Biological Conservation*, 193, 86–93. doi: 10.1016/J.BIOCON.2015.11.020

- 835 Puechmaille, S. J. (2016). The program structure does not reliably recover the correct population
836 structure when sampling is uneven: Subsampling and new estimators alleviate the problem.
837 *Molecular Ecology Resources*, 16(3), 608–627. doi: 10.1111/1755-0998.12512
- 838 Rašić, G., Filipović, I., Weeks, A. R., & Hoffmann, A. A. (2014). Genome-wide SNPs lead to strong signals
839 of geographic structure and relatedness patterns in the major arbovirus vector, *Aedes aegypti*. *BMC*
840 *Genomics*, 15(1), 275. doi: 10.1186/1471-2164-15-275
- 841 Ritchie, S. A., Moore, P., Carruthers, M., Williams, C., Montgomery, B., Foley, P., ... Russell, R. C. (2006).
842 Discovery of a Widespread Infestation of *Aedes albopictus* in the Torres Strait, Australia. *Journal of*
843 *the American Mosquito Control Association*, 22(3), 358–365. doi: 10.2987/8756-
844 971X(2006)22[358:DOAWIO]2.0.CO;2
- 845 Riveron, J. M., Irving, H., Ndula, M., Barnes, K. G., Ibrahim, S. S., Paine, M. J. I., & Wondji, C. S. (2013).
846 Directionally selected cytochrome P450 alleles are driving the spread of pyrethroid resistance in the
847 major malaria vector *Anopheles funestus*. *Proceedings of the National Academy of Sciences of the*
848 *United States of America*, 110(1), 252–257. doi: 10.1073/pnas.1216705110
- 849 Robinson, J. T., Thorvaldsdóttir, H., Winckler, W., Guttman, M., Lander, E. S., Getz, G., & Mesirov, J. P.
850 (2011, January 1). Integrative genomics viewer. *Nature Biotechnology*, Vol. 29, pp. 24–26. Nature
851 Publishing Group. doi: 10.1038/nbt.1754
- 852 Rousset, F. (2000). Genetic differentiation between individuals. *Journal of Evolutionary Biology*, 13(1),
853 58–62. doi: 10.1046/j.1420-9101.2000.00137.x
- 854 Schmidt, T. L., Chung, J., Honnen, A. C., Weeks, A. R., & Hoffmann, A. A. (2020). Population genomics of
855 two invasive mosquitoes (*Aedes aegypti* and *Aedes albopictus*) from the Indo-Pacific. *PLoS*
856 *Neglected Tropical Diseases*, 14(7), 1–24. doi: 10.1371/journal.pntd.0008463
- 857 Schmidt, T. L., Chung, J., van Rooyen, A. R., Sly, A., Weeks, A. R., & Hoffmann, A. A. (2020). Incursion
858 pathways of the Asian tiger mosquito (*Aedes albopictus*) into Australia contrast sharply with those
859 of the yellow fever mosquito (*Aedes aegypti*). *Pest Management Science*, 76(12), 4202–4209. doi:
860 10.1002/ps.5977
- 861 Schmidt, T. L., Filipović, I., Hoffmann, A. A., & Rašić, G. (2018). Fine-scale landscape genomics helps
862 explain the slow spatial spread of *Wolbachia* through the *Aedes aegypti* population in Cairns,

- 863 Australia. *Heredity*, 120(5), 386–395. doi: 10.1038/s41437-017-0039-9
- 864 Schmidt, T. L., Rašić, G., Zhang, D., Zheng, X., Xi, Z., & Hoffmann, A. A. (2017). Genome-wide SNPs reveal
865 the drivers of gene flow in an urban population of the Asian Tiger Mosquito, *Aedes albopictus*. *PLOS*
866 *Neglected Tropical Diseases*, 11(10), e0006009. doi: 10.1371/journal.pntd.0006009
- 867 Schmidt, T. L., van Rooyen, A. R., Chung, J., Endersby-Harshman, N. M., Griffin, P. C., Sly, A., ... Weeks, A.
868 R. (2019). Tracking genetic invasions: Genome-wide single nucleotide polymorphisms reveal the
869 source of pyrethroid-resistant *Aedes aegypti* (yellow fever mosquito) incursions at international
870 ports. *Evolutionary Applications*, 12(6), 1136–1146. doi: 10.1111/eva.12787
- 871 Schultz, C. B., & Crone, E. E. (2001). Edge-mediated dispersal behavior in a prairie butterfly. *Ecology*,
872 82(7), 1879–1892. doi: 10.1890/0012-9658(2001)082[1879:EMDBIA]2.0.CO;2
- 873 Sharov, A. A., & Liebhold, A. M. (1998). Model of slowing the spread of gypsy moth (Lepidoptera:
874 Lymantriidae) with a barrier zone. *Ecological Applications*, 8(4), 1170–1179. doi: 10.1890/1051-
875 0761(1998)008[1170:MOSTSO]2.0.CO;2
- 876 Sherpa, S., Blum, M. G. B., Capblancq, T., Cumer, T., Rioux, D., & Després, L. (2019). Unravelling the
877 invasion history of the Asian tiger mosquito in Europe. *Molecular Ecology*, 28(9), 2360–2377. doi:
878 10.1111/mec.15071
- 879 Shi, S., Yuan, N., Yang, M., Du, Z., Wang, J., Sheng, X., ... Xiao, J. (2018). Comprehensive Assessment of
880 Genotype Imputation Performance. *Human Heredity*, 83(3), 107–116. doi: 10.1159/000489758
- 881 Trense, D., Schmidt, T. L., Yang, Q., Chung, J., Hoffmann, A. A., & Fischer, K. (2020). Anthropogenic and
882 natural barriers affect genetic connectivity in an Alpine butterfly. *Molecular Ecology*. doi:
883 10.1111/mec.15707
- 884 van den Hurk, A. F., Nicholson, J., Beebe, N. W., Davis, J., Muzari, O. M., Russell, R. C., ... Ritchie, S. A.
885 (2016). Ten years of the Tiger: *Aedes albopictus* presence in Australia since its discovery in the
886 Torres Strait in 2005. *One Health*, 2, 19–24. doi: 10.1016/J.ONEHLT.2016.02.001
- 887 Waters, J. M., Fraser, C. I., & Hewitt, G. M. (2013). Founder takes all: density-dependent processes
888 structure biodiversity. *Trends in Ecology & Evolution*, 28, 78–85. doi: 10.1016/j.tree.2012.08.024
- 889 Wright, S. (1943). Isolation by Distance. *Genetics*, 28(2), 114–138. doi: 10.1016/B978-0-12-374984-

890 0.00820-2

891 Wright, S. (1946). Isolation by distance under diverse systems of mating. *Genetics*, 31(1), 39–59.

892 Retrieved from <https://www.ncbi.nlm.nih.gov/pmc/articles/PMC1209315/pdf/39.pdf>

893 Yadav, S., Stow, A., & Dudaniec, R. Y. (2020). Microgeographic adaptation corresponds with elevational

894 distributions of congeneric montane grasshoppers. *Molecular Ecology*, mec.15739. doi:

895 10.1111/mec.15739

896 Zheng, X., Levine, D., Shen, J., Gogarten, S. M., Laurie, C., & Weir, B. S. (2012). A high-performance

897 computing toolset for relatedness and principal component analysis of SNP data. *Bioinformatics*,

898 28(24), 3326–3328. doi: 10.1093/bioinformatics/bts606

899

900

901 **Figure Captions**

902

903 **Fig 1:** Locations and genetic structure of the TSI villages. A:Keriri, B:St Pauls (Moa Island) C:Kubin

904 (Moa Island), D:Badu, E:Mabuiag, F:Iama, G:Warraber, H:Poruma, I:Masig, J:Ugar, K:Erub, L:Mer.

905 Plots are of sparse non-negative matrix factorisation (sNMF) on the Region22 dataset (see

906 Datasets and filtering), and are centred over each village. Grey and blue sections of each vertical

907 bar represent ancestral lineages of individuals, assuming $K = 2$. White-dotted circles and black-

908 dotted squares of the same colour indicate close kin dyads found across villages, with squares

909 denoting the origin (see Table 2). The white crossed square indicates Dauan. The “x” indicates

910 Ngurapai, where the four incursive mosquitoes were detected. Map inset shows the Australian

911 mainland, Papua New Guinea (PNG) and the Torres Strait Islands (TSI). Maps produced in QGIS

912 (v3.6) using the Torres Strait Clear sky Landsat ([https://eatlas.org.au/data/uuid/71c8380e-4cdc-](https://eatlas.org.au/data/uuid/71c8380e-4cdc-4544-98b6-8a5c328930ad)

913 [4544-98b6-8a5c328930ad](https://eatlas.org.au/data/uuid/71c8380e-4cdc-4544-98b6-8a5c328930ad)) and the Bright Earth eAtlas basemap v1.0

914 (<https://eatlas.org.au/data/uuid/ac57aa5a-233b-4c2c-bd52-1fb40a31>). See Figures S1-S13 for

915 village maps and sampling point locations, and Figures S15-S17 for sNMF results for $2 \leq K \leq 4$.

916
917
918
919
920
921
922
923
924
925
926
927
928
929
930
931
932
933
934
935
936
937
938
939

Fig 2: Predicted locations of the four incursives from 1000 bootstrapping runs of Locator. Each prediction is depicted with a red circle. The “x” indicates Ngurapai, where the incursives were detected. The dotted line describes the position of the *cordon sanitaire*. See main text for point estimates of locations.

Fig 3: FineRADstructure coancestry map and tree. The left hand side panel indicates genotype sampling locations coloured by geographical proximity and with all non-TSI genotypes labelled. The central panel shows coancestry between genotypes, with light yellow indicating low coancestry, and darker yellows, oranges and reds indicating progressively higher coancestry. Solid black squares indicate the two major clades of TSI/Indonesia/Timor-Leste (top right) and all other genotypes (bottom left). Dashed squares indicate subgroups of PNG/Vanuatu, East Asia/Southeast Asia/Fiji, and Indonesia/Timor-Leste. The dotted square indicates J:Ugar, the only TSI village resolved into a single lineage. Blue asterisks indicate higher coancestry between PNG and TSI genotypes, particularly those from L:Mer. See Figure S31 for full-size figure.

940

941

942 **Tables**

943

944 Table 1: TSI village details and population genetic parameter estimates including
 945 heterozygosity (H_0) and nucleotide diversity (π) at variant sites, Tajima's D , Rousset's α for dyads
 946 < 50 m and > 500 m apart, and number of private alleles with and without inclusion of PNG
 947 samples.

Village key (Fig 1)	Village	Island area (km ²)	Human pop size (2016)	H_0 (\pm SE)	π (\pm SE)	Tajima's D (\pm SE)	Mean Rousset's α : <50m (\pm SD)	Mean Rousset's α : >500m (\pm SD)	Private alleles (no PNG)	Private alleles (PNG)
A	Keriri	14.5	268	0.063 (\pm 0.001)	0.074 (\pm 0.001)	-1.164 (\pm 0.026)	0.25 (\pm 0.07)	0.20 (\pm 0.10)	118	98
B	St Pauls (Moa)	152.4	248	0.063 (\pm 0.001)	0.074 (\pm 0.001)	-1.010 (\pm 0.030)	0.18 (\pm 0.08)	0.20 (\pm 0.10)	123	91
C	Kubin (Moa)	152.4	198	0.064 (\pm 0.001)	0.075 (\pm 0.001)	-0.809 (\pm 0.032)	0.16 (\pm 0.09)	0.16 (\pm 0.08)	97	80
D	Badu	101.9	813	0.065 (\pm 0.001)	0.078 (\pm 0.001)	-1.164 (\pm 0.028)	0.18 (\pm 0.07)	0.21 (\pm 0.09)	56	42
E	Mabuiag	6.3	210	0.065 (\pm 0.001)	0.076 (\pm 0.001)	-0.986 (\pm 0.028)	0.15 (\pm 0.11)	0.19 (\pm 0.06)	146	115
F	Iama	1.5	319	0.063 (\pm 0.001)	0.074 (\pm 0.001)	-0.691 (\pm 0.034)	0.21 (\pm 0.08)	0.12 (\pm 0.07)	120	85
G	Warraber	0.6	245	0.066 (\pm 0.001)	0.078 (\pm 0.001)	-0.980 (\pm 0.027)	0.20 (\pm 0.06)	0.23 (\pm 0.05)	77	66
H	Poruma	0.4	167	0.065 (\pm 0.001)	0.076 (\pm 0.001)	-0.972 (\pm 0.028)	0.17 (\pm 0.08)	0.19 (\pm 0.07)	105	83

I	Masig (2018)	1.5	270	0.069 (±0.001)	0.080 (±0.001)	-1.054 (±0.027)	0.11 (±0.00)	0.19 (±0.05)	128	90
I	Masig (2019)			0.073 (±0.001)	0.082 (±0.001)	-0.908 (±0.029)	0.14 (±0.02)	0.14 (±0.04)		
J	Ugar	0.4	85	0.063 (±0.001)	0.074 (±0.001)	-1.106 (±0.029)	0.22 (±0.06)	0.19 (±0.05)	130	85
K	Erub	6.9	328	0.063 (±0.001)	0.076 (±0.001)	-1.209 (±0.027)	0.19 (±0.09)	0.24 (±0.08)	182	123
L	Mer	4.3	450	0.067 (±0.001)	0.081 (±0.001)	-1.240 (±0.026)	0.22 (±0.10)	0.25 (±0.09)	148	77

948 Table 2: Putative close kin dyads within and across villages. Within villages, the dyad at
949 E:Mabuiag had the lowest PC-Relate kinship coefficient of the three close kin dyads, so this was
950 used as the cut-off for designating close kin across villages. Mean kinship describes the mean of
951 kinship coefficients between Sib-1 and Sib-2 and all other individuals from that village, using
952 kinship coefficients from the 3 PC treatment. Higher mean kinship in Village-2 shows this is the
953 origin.

Sib-1	Sib-2	Origin	Distance (km)	Kinship (KING)	Kinship (PC-Relate 3 PCs)	Kinship (PC-Relate 10 PCs)	Mean kinship Village-1 (±SD)	Mean kinship Village-2 (±SD)
Within villages								
K:Erub	K:Erub		0.17	0.43	0.59	0.47		
B:St Pauls	B:St Pauls		0	0.42	0.51	0.48		
E:Mabuiag	E:Mabuiag		0	0.34	0.32	0.28		
Between villages								
C:Kubin	A:Keriri	A:Keriri	35.26		0.52	0.35	-0.015 (±0.017)	0.042 (±0.038)
H:Poruma	G:Warraber	G:Warraber	31.51		0.51	0.41	-0.017 (±0.017)	0.032 (±0.033)

C:Kubin	B:St Pauls	B:St Pauls	13.50	0.49	0.46	-0.036 (±0.018)	0.001 (±0.021)
L:Mer	E:Mabuiag	E:Mabuiag	202.63	0.44	0.42	-0.013 (±0.018)	0.055 (±0.052)
B:St Pauls	E:Mabuiag	E:Mabuiag	30.59	0.44	0.44	-0.002 (±0.016)	0.060 (±0.040)

954

955

956

957

958

959

960 Table 3: Frequencies of non-reference alleles (p) at the four outlier SNPs on scaffold

961 NW_021838465.1. RADtag1 had one outlier SNP (pos: 84554160), RADtag2 had three outlier

962 SNPs (pos: 84888984, 84888990, 84888991) which always cooccurred except in case of missing

963 data. See Table S3 for a list of genes of known function within this region and Tables S7-S8 for

964 genotypes of all individuals at the four outlier SNPs.

965

	p(84554160)	p(84888984)	p(84888990)	p(84888991)
Location	RADtag1	RADtag2	RADtag2	RADtag2
TSI				
A:Keriri	0.056	0.045	0.045	0.045
I:Masig (2018)	0.238	0.272	0.272	0.272
I:Masig (2019)	0.250	0.250	0.250	0.250
L:Mer	0.040	0.021	0.021	0
J:Ugar	0	0.042	0.042	0.042
All other locations	0	0	0	0
International				

Port Moresby	0.235	0.265	0.282	0.265
Singapore	0.071	0	0	0
All other locations	0	0	0	0

966

967

968 **Supporting Information Legends**

969

970 **Text**

971 Text S1: Details of the genotyping pipeline.

972

973

974 **Tables**

975 Table S1: Initial assignPOP run showing assignment probability to each TSI and non-TSI location,
976 and aggregated assignment probabilities for all TSI and all non-TSI locations.

977 Table S2: Pairwise F_{ST} estimates among TSI villages.

978 Table S3: The first of four genomic regions containing multiple outlier SNPs found on multiple
979 RADtags, and the genes of known product or function located between these RADtags.

980 Table S4: The second of four genomic regions containing multiple outlier SNPs found on
981 multiple RADtags, and the genes of known product or function located between these RADtags.

982 Table S5: The third of four genomic regions containing multiple outlier SNPs found on multiple
983 RADtags, and the genes of known product or function located between these RADtags.

984 Table S6: The fourth of four genomic regions containing multiple outlier SNPs found on multiple
985 RADtags, and the genes of known product or function located between these RADtags.

986 Table S7: Non-reference alleles at the four outlier SNPs in Region 1 (see Table S2) found in TSI
987 villages.

988 Table S8: Non-reference alleles at the four outlier SNPs in Region 1 (see Table S2) found in non-
989 TSI locations.

990

991

992 **Figures**

993 Figure S1: Locations of *Aedes albopictus* sweep net collections on Badu Island. Map produced
994 using Mapinfo (2019) with the Queensland basemap satellite imagery (2020).

995 Figure S2: Locations of *Aedes albopictus* sweep net collections on Dauan Island. Map produced
996 using Mapinfo (2019) with the Queensland basemap satellite imagery (2020).

997 Figure S3: Locations of *Aedes albopictus* sweep net collections on Erub Island. Map produced
998 using Mapinfo (2019) with the Queensland basemap satellite imagery (2020).

999 Figure S4: Locations of *Aedes albopictus* sweep net collections on Iama Island. Map produced
1000 using Mapinfo (2019) with the Queensland basemap satellite imagery (2020).

1001 Figure S5: Locations of *Aedes albopictus* sweep net collections on Keriri Island. Map produced
1002 using Mapinfo (2019) with the Queensland basemap satellite imagery (2020).

1003 Figure S6: Locations of *Aedes albopictus* sweep net collections on Mabuiag Island. Map
1004 produced using Mapinfo (2019) with the Queensland basemap satellite imagery (2020).

1005 Figure S7: Locations of *Aedes albopictus* sweep net collections on Masig Island. Map produced
1006 using Mapinfo (2019) with the Queensland basemap satellite imagery (2020).

1007 Figure S8: Locations of *Aedes albopictus* sweep net collections on Poruma Island. Map produced
1008 using Mapinfo (2019) with the Queensland basemap satellite imagery (2020).

1009 Figure S9: Locations of *Aedes albopictus* sweep net collections on Mer Island. Map produced
1010 using Mapinfo (2019) with the Queensland basemap satellite imagery (2020).

1011 Figure S10: Locations of *Aedes albopictus* sweep net collections on Ugar Island. Map produced
1012 using Mapinfo (2019) with the Queensland basemap satellite imagery (2020).

1013 Figure S11: Locations of *Aedes albopictus* sweep net collections on St Pauls (Moa Island). Map
1014 produced using Mapinfo (2019) with the Queensland basemap satellite imagery (2020).

1015 Figure S12: Locations of *Aedes albopictus* sweep net collections on Kubin (Moa Island). Map
1016 produced using Mapinfo (2019) with the Queensland basemap satellite imagery (2020).

1017 Figure S13: Locations of *Aedes albopictus* sweep net collections on Warraber Island. Map
1018 produced using Mapinfo (2019) with the Queensland basemap satellite imagery (2020).

1019 Figure S14: Location of sweep net sampling sites and detected incursions on Ngurapai between
1020 2019-02-02 and 2019-02-09. Map produced using Mapinfo (2019) with the Queensland
1021 basemap satellite imagery (2020).

1022 Figure S15: Individual ancestral lineage proportions for each village (n=22) with two ancestral
1023 lineages (K = 2) selected.

1024 Figure S16: Individual ancestral lineage proportions for each village (n=22) with three ancestral
1025 lineages (K = 3) selected.

1026 Figure S17: Individual ancestral lineage proportions for each village (n=22) with four ancestral
1027 lineages (K = 4) selected.

1028 Figure S18: Scatter plot of a mantel test between geographic (natural log) and genetic distance
1029 (Rousset's a) for *Aedes albopictus* collections on Badu Island. Lines describe a linear regression
1030 fit with 95% Confidence Interval shown.

1031 Figure S19: Scatter plot of a mantel test between geographic (natural log) and genetic distance
1032 (Rousset's a) for *Aedes albopictus* collections on Keriri Island. Lines describe a linear regression
1033 fit with 95% Confidence Interval shown.

1034 Figure S20: Scatter plot of a mantel test between geographic (natural log) and genetic distance
1035 (Rousset's a) for *Aedes albopictus* collections on Masig Island in 2018. Lines describe a linear
1036 regression fit with 95% Confidence Interval shown.

1037 Figure S21: Scatter plot of a mantel test between geographic (natural log) and genetic distance
1038 (Rousset's a) for *Aedes albopictus* collections on Masig Island in 2019. Lines describe a linear
1039 regression fit with 95% Confidence Interval shown.

1040 Figure S22: Scatter plot of a mantel test between geographic (natural log) and genetic distance
1041 (Rousset's a) for *Aedes albopictus* collections on Mer Island. Lines describe a linear regression fit
1042 with 95% Confidence Interval shown.

1043 Figure S23: Scatter plot of a mantel test between geographic (natural log) and genetic distance
1044 (Rousset's a) for *Aedes albopictus* collections on Warraber Island. Lines describe a linear
1045 regression fit with 95% Confidence Interval shown.

1046 Figure S24: Scatter plot of a mantel test between geographic (natural log) and genetic distance
1047 (Rousset's a) for *Aedes albopictus* collections on Erub Island. Lines describe a linear regression
1048 fit with 95% Confidence Interval shown.

1049 Figure S25: Scatter plot of a mantel test between geographic (natural log) and genetic distance
1050 (Rousset's a) for *Aedes albopictus* collections on Mabuiag Island. Lines describe a linear
1051 regression fit with 95% Confidence Interval shown.

1052 Figure S26: Scatter plot of a mantel test between geographic (natural log) and genetic distance
1053 (Rousset's a) for *Aedes albopictus* collections on Poruma Island. Lines describe a linear
1054 regression fit with 95% Confidence Interval shown.

1055 Figure S27: Scatter plot of a mantel test between geographic (natural log) and genetic distance
1056 (Rousset's a) for *Aedes albopictus* collections on Iama Island. Lines describe a linear regression
1057 fit with 95% Confidence Interval shown.

1058 Figure S28: Scatter plot of a mantel test between geographic (natural log) and genetic distance
1059 (Rousset's a) for *Aedes albopictus* collections on Ugar Island. Lines describe a linear regression
1060 fit with 95% Confidence Interval shown.

1061 Figure S29: Scatter plot of a mantel test between geographic (natural log) and genetic distance
1062 (Rousset's a) for *Aedes albopictus* collections on Kubin (Moa Island). Lines describe a linear
1063 regression fit with 95% Confidence Interval shown.

1064 Figure S30: Scatter plot of a mantel test between geographic (natural log) and genetic distance
1065 (Rousset's a) for *Aedes albopictus* collections on St Pauls (Moa Island). Lines describe a linear
1066 regression fit with 95% Confidence Interval shown.

1067 Figure S31: Full-size figure of Fig 3.

1068 Figure S32: PCA-UMAP of all non-incurive genotypes, using the first 4 PCs, 50 neighbours and a
1069 0.5 minimum distance.

1070 Figure S33: Scree plot from pcadapt.

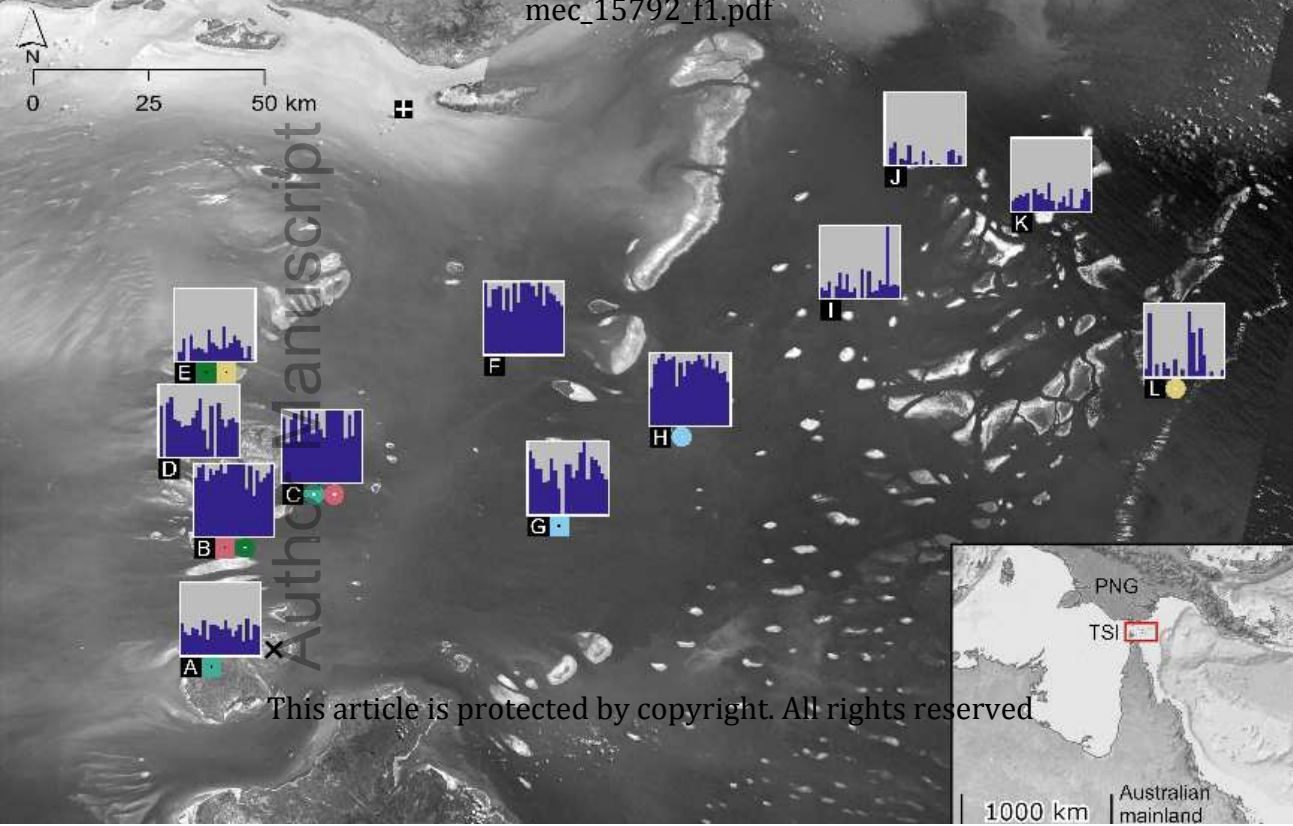
1071 Figure S34: Genome-wide genetic structure of TSI villages, for the first and second PCs.

1072 Figure S35: Genome-wide genetic structure of TSI villages, for the third and fourth PCs.

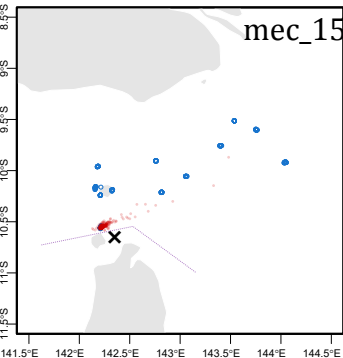
1073 Figure S36: Genome-wide genetic structure of TSI villages, for the fifth and sixth PCs.

1074 Figure S37: Genome-wide genetic structure of TSI villages, for the seventh and eighth PCs.

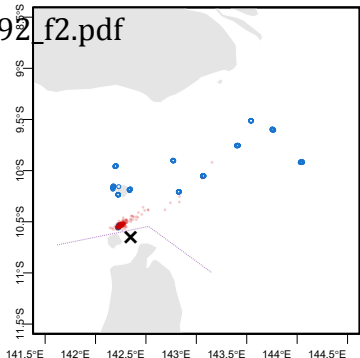
Author Manuscript



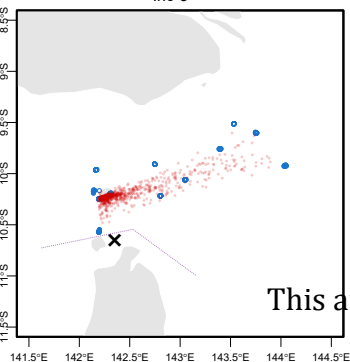
Inc-1



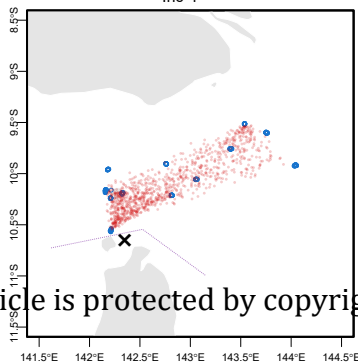
Inc-2



Inc-3



Inc-4



This article is protected by copyright

● Training Locations ● Predicted Locations

Timor-Leste Jakarta and Bandung Bali Japan Taiwan Guangzhou Singapore Port Moresby Madang Vanuatu

